JACS
JOURNAL OF THE AMERICAN CHEMICAL SOCIETY
Article
pubs.acs.org/JACS

Structural Insights into a Unique Inhibitor Binding Pocket in Kinesin Spindle Protein

Venkatasubramanian Ulaganathan,[§,†,‡] Sandeep K. Talapatra,[§,‡] Oliver Rath,[§] Andrew Pannifer,[∥] David D. Hackney,*[,⊥] and Frank Kozielski*[,§]

[§]The Molecular Motors Laboratory, The Beatson Institute for Cancer Research, Garscube Estate, Switchback Road, Glasgow G61 1BD, Scotland, U.K.

[∥]Drug Discovery Programme, The Beatson Institute for Cancer Research, Garscube Estate, Switchback Road, Glasgow G61 1BD, Scotland, U.K.

[⊥]Department of Biological Sciences, Carnegie Mellon University, 4400 Fifth Avenue, Pittsburgh, Pennsylvania 15213, United States

Supporting Information

ABSTRACT: Human kinesin Eg5 is a target for drug development in cancer chemotherapy with compounds in phase II clinical trials. These agents bind to a well-characterized allosteric pocket involving the loop L5 region, a structural element in kinesin-5 family members thought to provide inhibitor specificity. Using X-ray crystallography, kinetic, and biophysical methods, we have identified and characterized a distinct allosteric pocket in Eg5 able to bind inhibitors with nanomolar K_d. This pocket is formed by key structural elements thought to be pivotal for force generation in kinesins and may represent a novel site for therapeutic intervention in this increasingly well-validated drug target.

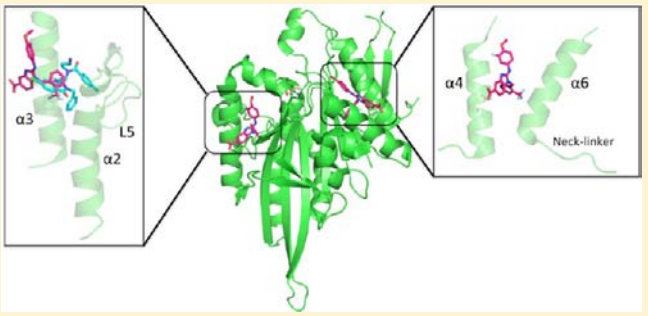

1. INTRODUCTION

The kinesins are a superfamily of molecular motors that play a key role in a diverse range of physiological functions by transporting intracellular cargos along microtubule (MT) filaments. Sometimes described as "nano-machines", kinesins convert the chemical energy of ATP into mechanical force, driving their cargos in most cases toward the plus end of the MT. Several kinesins play a critical role in the cell cycle. Eg5 (also known as KSP and a member of the kinesin-5 subfamily) is required to form the mitotic spindle and inhibition of Eg5 results in distinctive monoastral spindles, cell cycle arrest and cell death. Consequently, there is growing interest in the kinesins as targets for cancer chemotherapy and there are now potent inhibitors for two kinesin superfamily members, Eg5 and CENP-E, in phase I and II clinical trials.[1−4] The most advanced drug target of the kinesin superfamily is Eg5 for which there are several highly specific inhibitors in clinical development such as ispinesib, SB-743921 and ARRY-520. Without exception they all target an extensively studied allosteric site about 10 Å away from the ATP binding pocket in a region formed by helix α2/loop L5 and helix α3.[5] These inhibitors show potent in vivo activity but drug-resistant mutants have already been identified in cell culture. The nucleotide-binding pocket of kinesins has also been targeted for drug development through ATP-competitive inhibitors,[6,7] without binding to the ATP site, and the existence of other putative sites on Eg5 for intervention has been predicted by molecular modeling techniques.[8] The identification of a novel inhibitor-binding pocket presents the opportunity to develop new series of inhibitors that could be used either alone or in combination with existing Eg5 compounds. Using a benzimidazole series of Eg5 inhibitors that was shown to bind to the enzyme in the presence of ispinesib,[9] we have used X-ray crystallography to characterize an allosteric pocket formed by helices α4 and α6. Unexpectedly, we found that these inhibitors also bind to the known ispinesib pocket, and using Isothermal Titration Calorimetry (ITC), Surface Plasmon Resonance (SPR), classical enzyme kinetics and cell-based assays, we show that the observed inhibition by the inhibitor is due to its binding at the novel site and that binding at the ispinesib site is very weak.

2. MATERIALS AND METHODS

Characterization and Purity of BI8. BI8 was synthesized in six steps as previously described (Supporting Information section and Scheme S1).[10] The compound was judged to be 94.1% pure from LC−MS. ^{1}H NMR (400 MHz, MeOD) δ 8.12 ppm (s, 1H), 7.73 (d, J = 8.4 Hz, 2H), 7.49 (m, 3H), 7.25−7.28(m 2H), 7.05 (t, J = 9.1 Hz, 1H), 6.91 (d, J = 8.3 Hz, 1H), 6.74 (d, J = 17.4 Hz,1H), 5.66 (s, 2H), 4.84(s, 1H), 3.83(s, 3H). ^{19}F NMR (376 MHz, MeOD) Φ −61.55 (s), −135.38 (s). ^{13}C NMR (125 MHz, MeOD): δ 169.35, 152.98, 152.39, 143.21, 140.44, 136.32, 133.78, 133.15, 133.05, 132.08, 127.23, 126.82, 126.52, 125.69, 124.91, 122.75, 122.24, 117.18, 115.39, 113.59, 106.88

Received: October 20, 2012
Published: January 10, 2013

   dx.doi.org/10.1021/ja310377d | J. Am. Chem. Soc. 2013, 135, 2263−2272

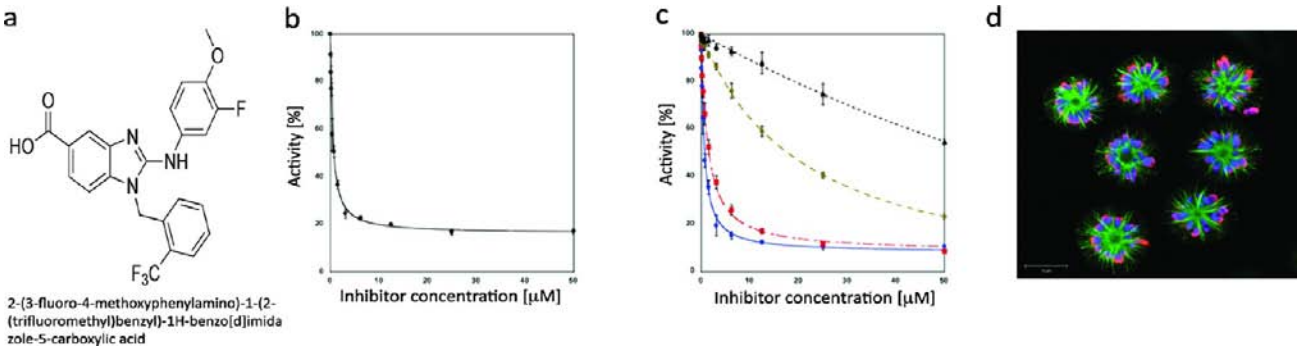

Figure 1. Biochemical characterization of the Eg5-BI8 complex. (a) Chemical structure and systematic name of the benzimidazole-based Eg5 inhibitor BI8. (b) Concentration−response plots for the inhibition of the basal (IC_{50} = 458.8 ± 28.3 nM) and (c) MT-stimulated Eg5 ATPase activities at 150 mM NaCl (IC_{50} = 590.2 ± 26.0 nM; blue circles), 100 mM NaCl (1.3 ± 0.1 μM; red), 50 mM (20.9 ± 2.0 μM; olive) and without addition of salt (partial inhibition; black). (d) Induction of characteristic monoastral spindles by BI8 in HCT116 cells. Immunostaining of α-tubulin in green, phospho-Histon H3 in red and chromosomes in blue.

55.29, 47.08. HR-MS (*m*/*z*): [M]+ calculated for $C_{23}H_{17}N_3F_4O_3$, 460.1279; found, 460.1272. Analysis (% calculated, % found for $C_{23}H_{17}N_3F_4O_3$): C (60.13, 58.42), H (3.73, 3.74), N (9.15, 8.27).

Protein Crystallization. A total of 50 μL of Eg5 (10 mg/mL) was mixed carefully with 2 μL of BI8 (50 mM) and the mixture was incubated at 4 °C for 2 h. The mixture was then centrifuged at 13 000*g* for 5 min to remove any undissolved inhibitor. Diffraction quality single crystals of Eg5-BI8 complex were obtained by sitting drop, vapor diffusion using 1 μL of protein complex and 1 μL of the reservoir solution (0.1 M 4-(2-hydroxyethyl)-1-piperazinethanesulfonic acid (HEPES) buffer at pH 7.5, 20% (w/v) polyethylene glycol (PEG) 3350 and 0.1 M $MgCl_2$) in VDX plates (Hampton Research) at 19 °C. The crystal was cryoprotected using 0.12 M HEPES buffer at pH 7.5, 22% (w/v) PEG 3350, 0.12 M $MgCl_2$ and 15% (v/v) PEG-400 and flash frozen in liquid nitrogen.

Data Collection and Refinement. Data were collected at Diamond Light Source at beamline I02 and processed using XDS.[11] The integrated data were scaled using SCALA. The Eg5-BI8 complex belonged to space group *C*2 with one molecule in the asymmetric unit. The structure was solved by molecular replacement (Molrep[12]) using a single chain of Eg5 in complex with STLC (PDB ID 2WOG). A single subunit was positioned and refined using REFMAC5[13] and PHENIX refine.[14] The R_{free} was calculated by using 5% of data. The σA weighted electron density map and difference map were inspected and the model was improved using COOT.[15] The ligand coordinates and cif dictionaries were prepared using the PRODRG server.[16] Data collection and refinement statistics are given in Table S1. The structure is very well refined with an R_{free} of 23.3% with 97.6% of all residues in the preferred region of the Ramachandran plot, 1.7% in the allowed region and 0.7% outliers. The final model comprises residues 18−363, one molecule of Mg^{2+}ADP, one HEPES moiety and two BI8 molecules. Residues 1−17 preceding the motor domain, 174−181 (loop L7) and 272−286 (loop L11) are missing due to high flexibility in these regions. Mg^{2+}ADP is bound in the nucleotide-binding region with the Mg ion being octahedrally coordinated. Figures were prepared using Pymol.[17] Coordinates and structure factors of the Eg5-BI8 complex have been deposited with the PDB under 3ZCW.

Surface Plasmon Resonance Competition Assays. Experiments were performed at 25 °C using a Biacore T100 (Biacore) in running buffer (50 mM TRIS, pH 7.0, 200 mM NaCl, 1 mM $MgCl_2$, 0.5 mM EDTA and 0.05% surfactant P20) supplemented with 1% DMSO before each run with a flow rate of 30 μL/min. Experiments were performed at least in duplicate. Double His-tagged Eg5 (200 nM) was immobilized on the surface of the NTA sensor chip charged with Ni^{2+} to approximately 2000 RU. The sensor surface was regenerated between each experiment with a 60 and 120 s injection of 1 M Imidazole and 10 mM HEPES, pH 8.3, 150 mM NaCl, 350 mM EDTA and 0.005% P20, respectively. For analyte preparation, the compounds were prepared in DMSO as a 50 mM stock solution. Concentration series for each inhibitor were prepared ensuring a consistent final DMSO concentration of 1%. To correct for the minor DMSO volume effect, a DMSO calibration series was prepared using 0.5% and 1.8% of DMSO in running buffer. A set of 8 aliquots of 700 μL each was prepared using the two DMSO concentrations for the DMSO standard curve. Protein immobilization on the chip was carried out at a flow rate of 5 μL/min, whereas for the experiments, a flow rate of 30 μL/min was used. The steady state analyses of molecular interactions were calculated after subtraction of backgrounds (inhibitor binding to a control flow cell) using the BIAcore T100 Evaluation software and Kaleidagraph 4.0. The binding constant K_D was determined according to the respective binding model. To investigate two-site binding and to analyze the affinity for both sites, BI8 was measured in a range from 0 to 528 μM. BI8 was first injected to determine the binding affinity of the two sites followed by a single ispinesib injection at 10 μM. As hypothesized, ispinesib competitively removed BI8 from the allosteric pocket saturating the site at a concentration of 10 μM. BI8 was then injected at the same range to determine the K_D for the second novel site. Similarly, as a negative control, monastrol was used at a concentration series ranging from 0 to 40 μM. Two independent runs of 200 nM Eg5 immobilized at 2000 RU over the same NTA sensor surface charged with Ni^{2+} for 12 h had a loss of only ∼100−150 RU providing evidence for the stability of binding of double histidine tagged Eg5 ($Eg5_{1-368}$-12His) over time on the sensor surface. The sensorgram was allowed to proceed for a longer period after each injection to ensure that the injection had completely finished.

Biophysical Experiments. All fluorescence experiments were performed in A25 buffer with 25 mM KCl and 125 mM NaCl. Fluorescence spectra and titrations were performed at room temperature with a Tecan Saphire2 fluorimeter with band widths of 10 and 5 nm for excitation and emission. Transient experiments were performed with an Applied Photophysics SX20 stopped flow fluorimeter at 25 °C using excitation at 280 nm and a 305 nm long pass filter for intrinsic fluorescence of tyrosine and tryptophan.

3. RESULTS

A series of benzimidazole inhibitors of Eg5 were disclosed which were able to bind Eg5 in the presence of ispinesib,[9] suggesting the presence of a second binding site in the enzyme. We synthesized a set of benzimidazole analogues and determined their IC_{50} values for the inhibition of the basal and MT-stimulated ATPase activity. One particular compound, named BI8 (BenzImidazole number 8) (Figure 1a; Supplementary Methods and Scheme 1), demonstrated nanomolar potency inhibiting the basal ATPase activity (Figure 1b) and reasonable physicochemical properties. Interestingly, the IC_{50} for the inhibition of the MT-stimulated ATPase activity varied depending on the ionic strength (Figure 1c), a behavior

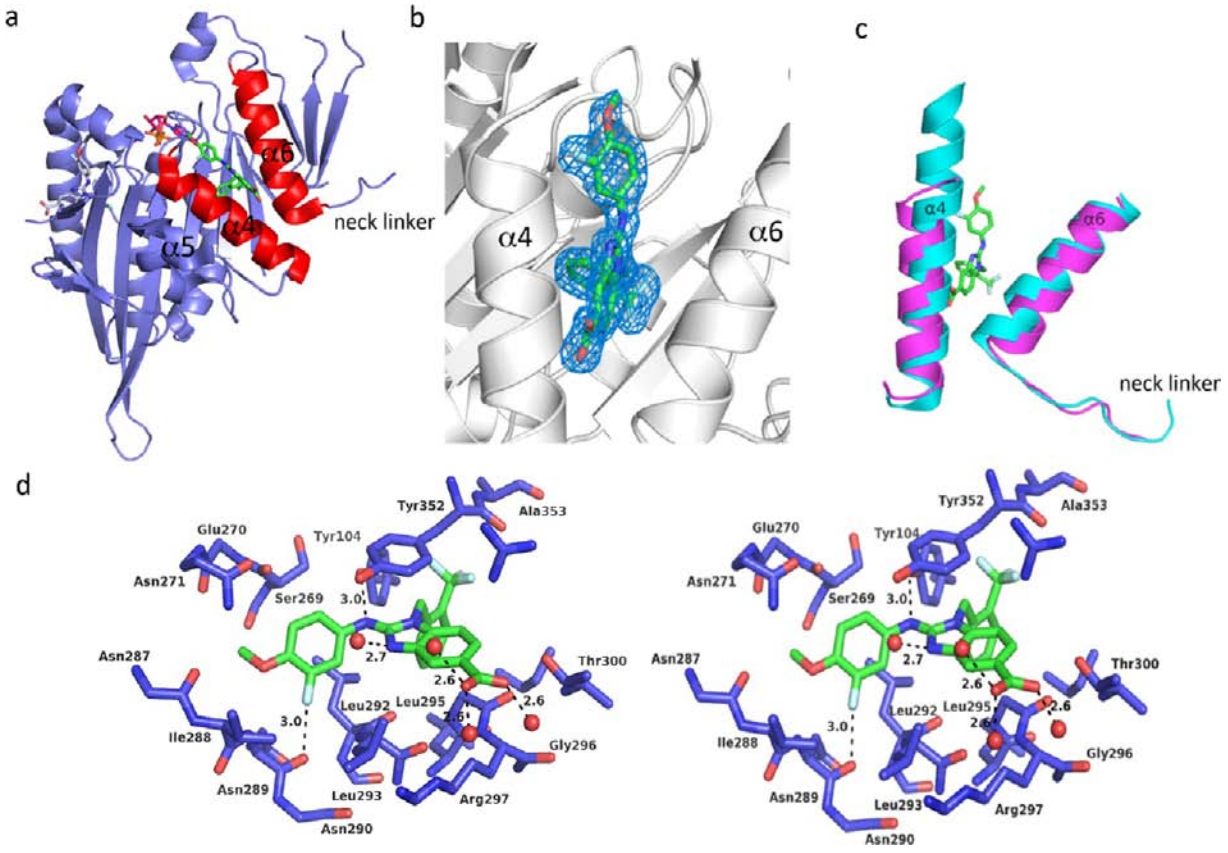

Figure 2. Characterization of the α4/α6 inhibitor-binding pocket in Eg5. (a) Back view of Eg5 showing the allosteric binding pocket occupied by BI8 (colored in green), formed by helix α4 of the switch II cluster and helix α6 (both colored in red), preceding the neck-linker. (b) Electron density omit map (colored in blue) contoured at 3 σ for BI8 bound in this pocket. (c) Conformational changes induced upon binding of BI8 in the helix α4/α6 pocket (purple), compared to native Eg5 (light blue). (d) Magnification of the inhibitor-binding pocket. BI8 is shown in green and residues forming the inhibitor-binding pocket are colored in purple. Water molecules are shown as red spheres and hydrogen-bond interactions are shown as dotted lines.

previously observed for monastrol and which was explained by altering the strength of the electrostatic interactions between the Eg5 motor and MTs.[18] In HCT116 cells, BI8 shows a GI_{50} value of 25 ± 3 μM, indicating weak cell permeability. BI8 induces monoastral spindles (Figure 1d), the typical phenotype observed for Eg5 inhibitors. To understand the novel binding characteristics of BI8 identified in kinetic experiments, we determined the structures of the Eg5-BI8 complex to 1.7 Å. Data collection and refinement statistics are summarized in Table S1. Clear well-defined electron density was observed for BI8 in a novel site but unexpectedly BI8 was also observed to bind in a pocket partially overlapping with the known ispinesib site.[19]

An Allosteric Inhibitor-Binding Site Formed by Helices α4 and α6. The BI8 inhibitor-binding pocket is formed by helix α4 of the switch II cluster, helix α6 preceding the neck-linker region and strand β3 (Figure 2a). The electron density map for the inhibitor is very well-defined with the entire molecule apparent (Figure 2b). Both helices α4 and α6 move outward by about 2 Å to accommodate the inhibitor (Figure 2c). The neck linker region is undocked but structured representing the intermediate inhibitor-bound state. The most striking feature of the complex between the inhibitor and residues of this binding pocket is the extensive network of aromatic interactions (Figure 2d): The side chain of Tyr352 forms a face-to-face stacking interaction with the benzimidazole ring while Tyr104 forms another face-to-face interaction with the trifluoromethylbenzyl group of the inhibitor. Analysis of the structure using the Glide module from the Schrodinger modeling software suite identified these aromatic residues as having particularly favorable interactions with the ligand. In addition, further hydrophobic interactions are formed. The 3-fluoro-4-methoxyphenyl group is within van der Waals distance of the side chain of Leu292 (α4) and Leu295 is buried upon binding of BI8. BI8 also forms a network of polar interactions to the protein and to solvent molecules. The carboxylate group makes a direct hydrogen bond interaction with Thr300 and also to a water molecule, mediating an interaction with the side chains of Arg297 (both helix α4). The solvent exposure of the carboxylate may attenuate the binding energy associated with these polar interactions but the interatomic distances are in the range expected for a strong hydrogen bond. The solvent-exposed nitrogen atom of the imidazole ring makes another water-mediated hydrogen bond interaction to the phenolic moiety of Tyr352. The amino group of the methoxyphenyl moiety forms a hydrogen bond interaction with the hydroxyl group of Tyr104 (β3). The 3-fluoro substituent of the methoxyphenyl group shows weak van der Waals interactions with the side chain of Ile288 and the main chain oxygen of Asn289 (both α4). Finally, the secondary amino group of BI8 forms a strong hydrogen bond interaction with the hydroxyl group of Tyr104 (β3) and a weak hydrogen bond is formed between the methoxy group of BI8 and Asn289.

dx.doi.org/10.1021/ja310377d | J. Am. Chem. Soc. 2013, 135, 2263−2272

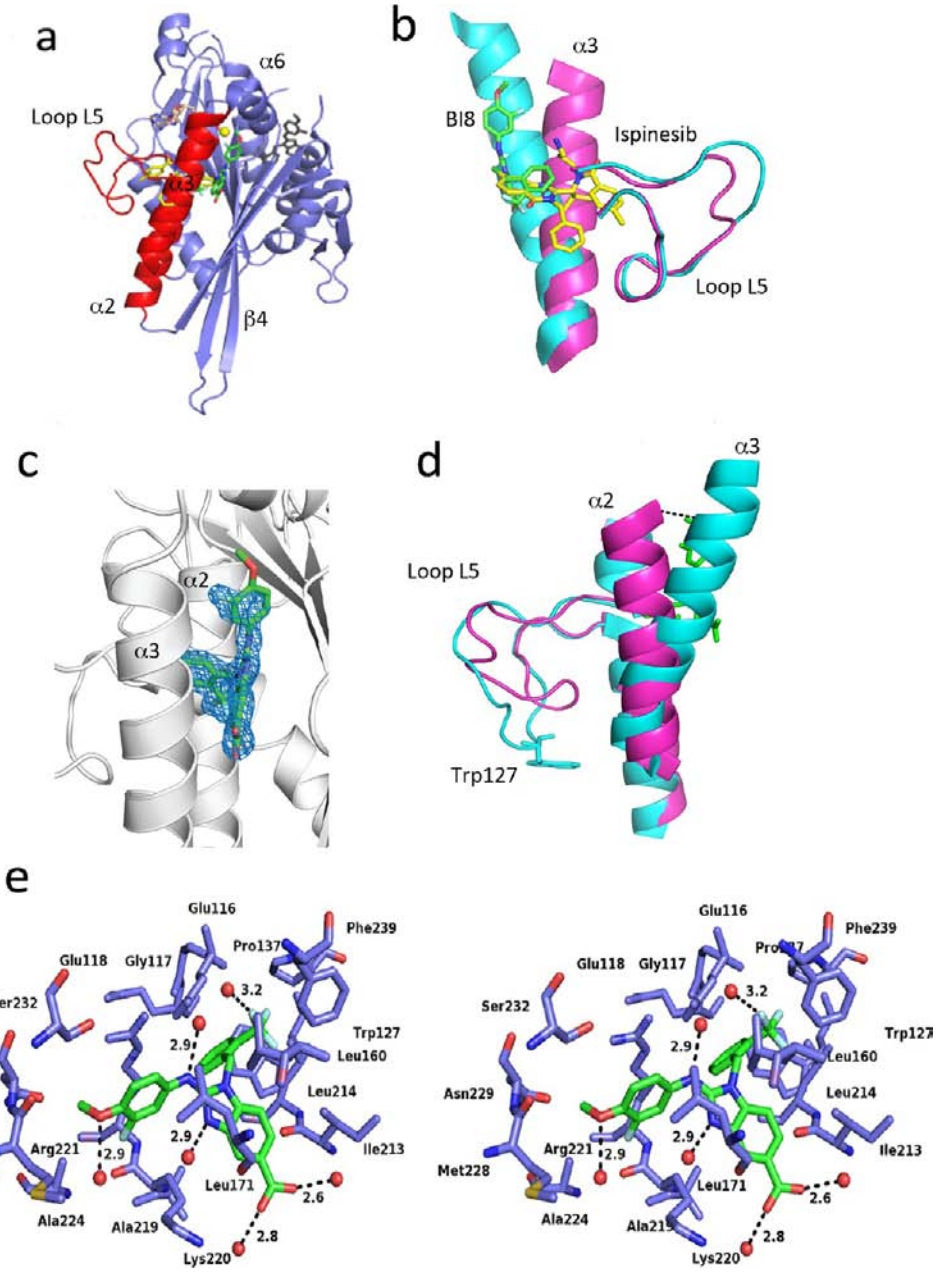

Figure 3. Characterization of the second allosteric binding pocket. (a) Eg5 in complex with Mg^{2+}ADP (pink) and BI8 (green) bound in the allosteric inhibitor-binding pocket formed by helices α2 and α3 and loops L7 as well as L9. BI8 bound in the novel site is colored in gray. (b) Overlay of Eg5-BI8 and Eg5-ispinesib complexes in the inhibitor-binding region. There is a significant overlap of BI8 (green color) with ispinesib (shaded in yellow). (c) $F_o - F_c$ omit map of BI8 bound in the inhibitor-binding pocket, contoured at 3σ (colored in blue). The methoxy group has no density in the omit map indicating that its position is flexible. (d) Binding of BI8 to the allosteric pocket leads to significant proximal structural changes in loop L5 and helix α3. (e) Stereoplot of the magnification of the inhibitor-binding pocket showing residues involved in BI8 binding.

The Second Inhibitor-Binding Site Overlaps with the Established Allosteric Ispinesib Pocket. The second pocket is formed by helices α2 and α3 and loops L7 and L9 (Figure 3a) and partially overlaps with the binding site of well-characterized Eg5 inhibitors such as ispinesib (Figure 3b) and monastrol. Electron density for this site appeared only toward the end of the refinement and parts of the molecule, such as the methoxy group, are disordered (Figure 3c) suggesting either greater flexibility or lower occupancy for BI8. Although loop L5 does not seem to be directly involved in inhibitor binding, it displays a new conformation that differs from the ones described for the native Eg5 structure or the conformation described for other Eg5-inhibitor bound complexes (Figure 3d). Trp127, which is solvent exposed in the native Eg5 structure, moves by 7.2 Å (C_α–C_α) and now interacts with Asp130 (loop L5) and Glu215 (α3). The upper part of helix α3 is rotated by approximately 14° around an axis close to the apex of the helix to accommodate the inhibitor leading to a shift of about 7 Å at the top of helix α3 (Figure 3d). These radical changes on BI8 binding have not been observed previously with any other Eg5 structure and are most likely due to BI8 binding. In contrast to the novel site, BI8 binding at this site does not demonstrate the network of aromatic interactions and this would be expected to reduce the binding energy by

dx.doi.org/10.1021/ja310377d | J. Am. Chem. Soc. 2013, 135, 2263−2272

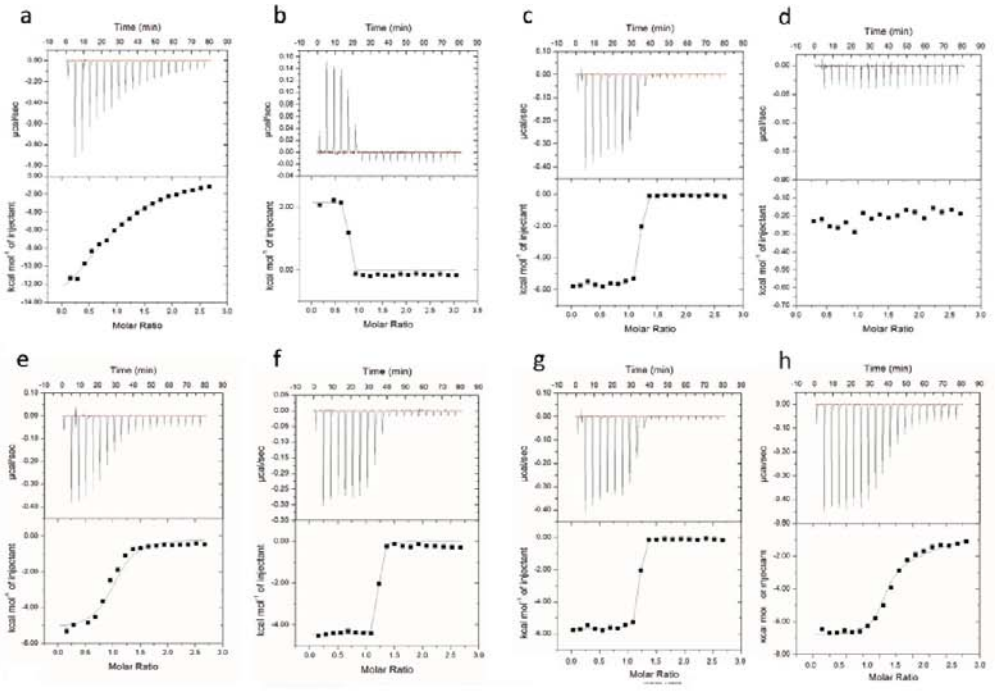

j

Preloaded mix	Ligand [μM]		n	ITC K_a[a] [μM]	ΔH[a] [kcal/mol]	TΔS[a] [kcal/mol]
Eg5, ADP	Ispinesib-Monastrol	Ispinesib	1.18 ± 0.07	<0.01	-5.82 ± 0.19	4.42 ± 0.32
		Monastrol	No binding			
Eg5, ADP	Monastrol-Ispinesib	Monastrol	0.93 ± 0.07	14.30 ± 0.64	-15.88 ± 0.37	-9.24 ± 0.40
		Ispinesib	0.78 ± 0.10	<0.01	2.22 ± 0.086	14.35 ± 0.78
Eg5, ADP	BI8-Ispinesib	BJ8 (1st site)	2	0.65 ± 0.01	-5.01 ± 0.23	3.18 ± 0.65
		BJ8 (2nd site)		27.53 ± 3.94	-4.68 ± 0.74	-10.25 ± 1.64
		Ispinesib	0.78 ± 0.22	<0.01	-5.16 ± 0.62	5.94 ± 1.37
Eg5, ADP	Ispinesib-BI8	Ispinesib	1.06 ± 0.03	<0.01	-4.12 ± 0.10	3.84 ± 0.01
		BJ8	1.22 ± 0.01	3.30 ± 0.66	-4.44 ± 0.11	3.04 ± 0.21

Figure 4. ITC analyses of ligand binding to Eg5. Raw isothermal titration calorimetry data (upper panels) and normalized ITC data for titrations plotted versus the molar ratio of titrant/protein (lower panels) demonstrating saturable exothermic and endothermic evolution of heat upon sequential additions of (a) monastrol (500 μM) and (b) ispinesib (500 μM) to Eg5. The reverse experiment was performed by sequential additions of (c) ispinesib (500 μM) and (d) monastrol (500 μM) to Eg5. Additions of (e) BI8 (500 μM) followed by (f) ispinesib (500 μM) to Eg5. The reverse experiment with sequential additions of (g) ispinesib (500 μM) and (h) BI8 (500 μM) to Eg5. (i) Thermodynamic cycle for ligand (ispinesib/monastrol) binding to Eg5, showing the relationship between the enthalpic changes of binding on monastrol, ispinesib and ispinesib competitively replacing monastrol from the allosteric binding site. (j) Summary of ITC data for BI8 in combination with two other Eg5-specific inhibitors, ispinesib and monastrol. Data analysis indicates that the binding data fit well to a two binding site model for BI8 and a single binding-site model for ispinesib.

comparison. There are some hydrophobic interactions, notably with the side chains of Leu160 and Leu172 and also a stacking interaction between Arg221 and the methoxybenzene group of BI8. Hydrogen bonding interactions are also present with the anilinic nitrogen forming a water-mediated hydrogen bond to Ser237. The 5-carboxylic acid group of the benzimidazole moiety is solvent exposed and displays several hydrogen bonds with nearby water molecules (Figure 3e) but these water molecules do not appear to mediate interaction with the protein.

The observation that BI8 binds at the known ispinesib site raises the possibility that the potent inhibition measured in biochemical assays could be due to binding at this site and the binding at the novel site could be weak. To distinguish which site was generating the potent inhibition, we used two label-free biophysical approaches and fluorescence techniques to

dx.doi.org/10.1021/ja310377d | J. Am. Chem. Soc. 2013, 135, 2263−2272

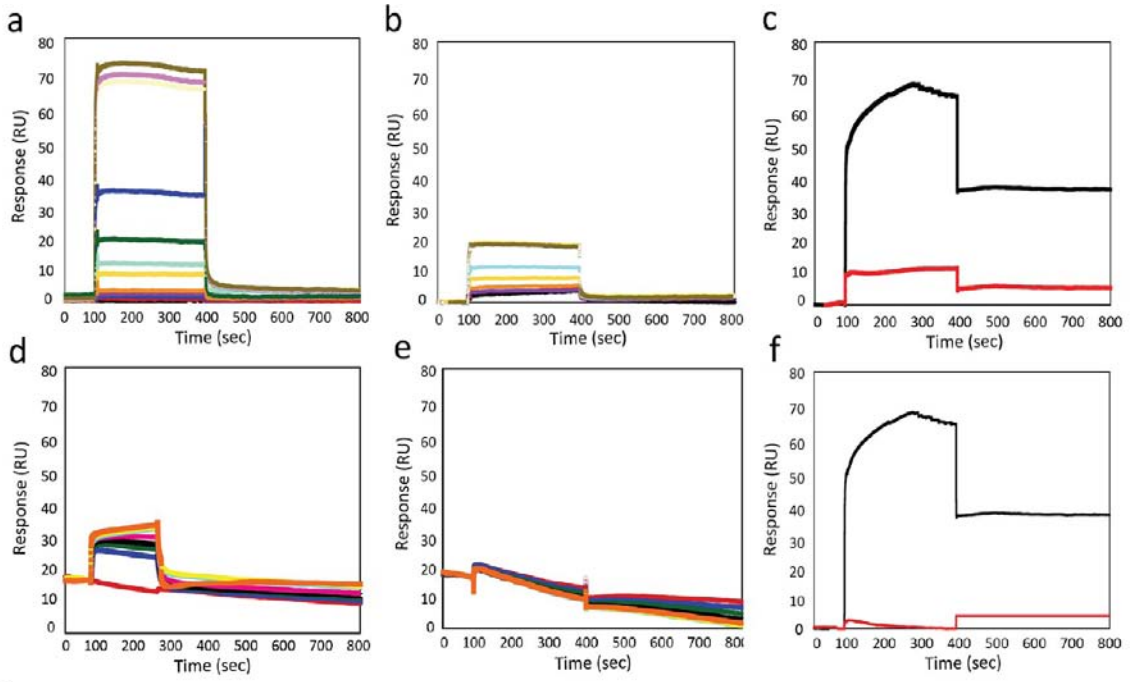

g

Inhibitor	K_{d1} (μM)	K_{d2} (μM)	$R_{max}1$	$R_{max}2$	χ^2
BI8 (before ispinesib injection)	0.47 ± 0.0002	34.4 ± 0.0045	40.2	70.8	10.5
BI8 (after ispinesib injection)	0.64 ± 0.092	---	20.5	---	4.5
Monastrol (before ispinesib injection)	1.28 ± 0.012	---	20.8	---	4.0
Monastrol (after ispinesib injection)	no inhibition	---	---	---	---

Figure 5. SPR competition studies of BI8, ispinesib and monastrol to double hexahistidine tagged Eg5 immobilized on NTA surface. (a) SPR response curves for increasing BI8 concentrations (0−528 μM) monitored on a surface with 2000 RU of double histidine tagged Eg5. (b) SPR response curves for various concentrations of BI8 from 0 to 528 μM monitored on a surface with 2000 RU of double histidine tagged Eg5 after injection of a saturating concentration of ispinesib indicating BI8 binding to a novel second site. (c) Ispinesib injection at 10 μM before (black) and after (red) second BI8 injection. The first ispinesib injection competitively removes BI8 from the mutual site which allows BI8 to bind only to the second novel site, whereas the second ispinesib injection with low or no response confirmed that ispinesib remains bound to Eg5 through second BI8 injection. d) SPR response curves for various concentrations of monastrol injection from 0 to 40 μM monitored on a surface with 2000 RU of double histidine tagged Eg5. (e) SPR response curves for various concentrations of second BI8 injection from 0 to 40 μM monitored on a surface with 2000 RU of double histidine tagged Eg5 after injection of a saturating concentration of ispinesib indicating that monastrol cannot bind due to its lower affinity compared to ispinesib to the same binding site. (f) Ispinesib injection at 10 μM before (black) and after (red) second monastrol injection. The first ispinesib injection competitively removes monastrol from the allosteric inhibitor site. Therefore, monastrol shows no response upon second injection. Second ispinesib injection with low or no response confirmed that ispinesib remains bound to Eg5 throughout second monastrol injection. (g) The table represents K_d for BI8 and monastrol binding, using the steady state affinity model, experimental R_{max} for each measurement and χ^2 distributions around 10 suggesting a good fit of the model to the experimental data. All measurements for SPR binding were reference corrected.

demonstrate that there is a single high affinity site and binding at this novel site accounted for the measured inhibition.

Isothermal Titration Calorimetry Competition Assays. To dissect the contribution made to the potent biochemical inhibition by each of the inhibitor-binding pockets, we investigated the interaction between Eg5 and BI8 using ITC competition assays. By blockading the ispinesib site using saturating concentrations of ispinesib and then titrating in BI8, the binding of BI8 to the novel pocket can be isolated and characterized thermodynamically. We first carried out a proof of principle experiment of this "ispinesib blockade" approach by testing whether ispinesib could block the binding of monastrol, a moderately potent inhibitor known to bind at the ispinesib site (Figure 4a−d). Monastrol was shown to bind the Eg5-ADP complex with a K_d of 1.4 μM, in agreement with recently published data. Monastrol binding exhibited a strong enthalpy contribution to the Gibbs Free Energy of binding. The K_d of ispinesib cannot be accurately estimated due to the step-like curve but is approximately 10 nM and is entropically dominated. In both cases, a 1:1, ligand/protein stoichiometry was observed, in agreement with existing crystal structures. We then saturated the Eg5-ADP complex with ispinesib and titrated monastrol into the saturated Eg5-ADP-ispinesib complex and observed no monastrol binding, consistent with the site being

dx.doi.org/10.1021/ja310377d | J. Am. Chem. Soc. 2013, 135, 2263−2272

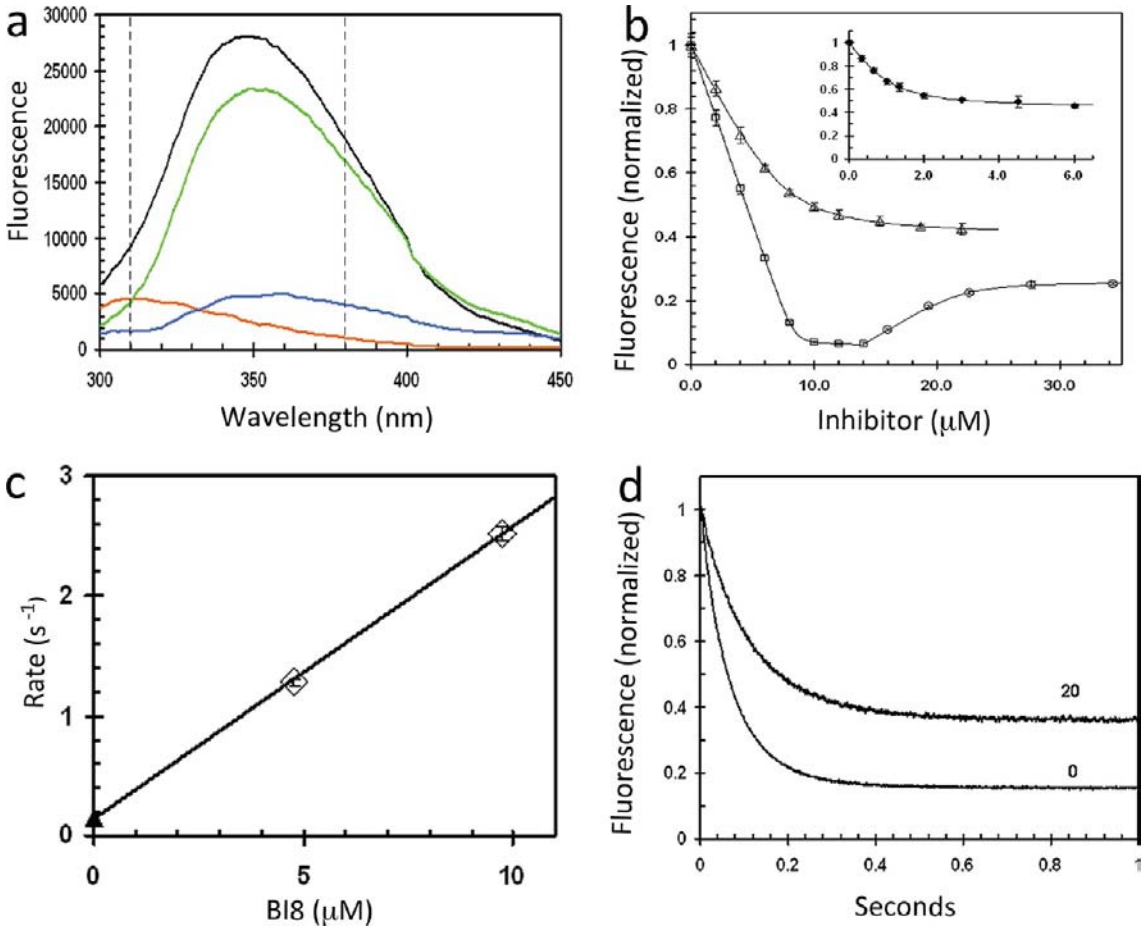

Figure 6. Intrinsic fluorescence titration of BI8 binding. (a) Emission spectra of Eg5 with BI8 and ispinesib. Spectra of 1.7 μM Eg5 with 0.2 mM ADP alone (black), 4 μM ispinesib (orange), 4 μM BI8 (green) or 4 μM ispinesib and 4 μM BI8 (blue). Excitation was at 280 nm. (b) Fluorescence titration of Eg5 with BI8 and ispinesib. Eg5 (6.4 μM) with 0.2 mM ADP was titrated with BI8 or ispinesib. Excitation was at 280 nm. Emission was at 310 nm for titration with BI8 alone (triangles) and at 380 nm for sequential addition of ispinesib (squares) followed by BI8 (circles). The theoretical curves were fit using the full quadratic expression for mutual depletion. (c) Kinetics of BI8 binding to Eg5. Eg5 with 0.2 mM ADP was mixed with BI8 for final concentrations of 0.5 μM Eg5 and 5 or 10 μM BI8. Excitation was at 280 nm with a 305 long pass emission filter. The first-order rate constant for the decrease in fluorescence on binding of BI8 is plotted versus the average concentration of free BI8 during the transient. The intercept on the *Y*-axis (solid triangle) is fixed at 0.14 s^{-1} for the dissociation rate constant. (d) Influence of BI8 on binding kinetics of ispinesib. Eg5 (1 μM) with 0.2 mM ADP and either 0 or 20 μM BI8 was mixed with an equal volume of 8 μM ispinesib. Excitation was at 280 nm with a 305 long pass emission filter.

inaccessible due to blockade by the more potent compound. We then performed the reverse experiment by saturating the Eg5-ADP complex with monastrol and titrating in ispinesib. As expected, ispinesib binding was observed, consistent with ispinesib displacing the weaker-binding monastrol. The endothermic binding observed in this second competition assay is also consistent with displacement of monastrol (Figure 4i). Having demonstrated the validity of the ispinesib blockade, we then investigated the binding of BI8 to the Eg5-ADP complex in the presence of ispinesib (Figure 4e–h).

First, we titrated in BI8, and obtained data that was best modeled using a sequential model with two sites in agreement with our crystal structure (Figure 4e). The data indicate the existence of one strong (K_d = 0.65 ± 0.01 μM) and one weaker (K_d = 27.5 ± 3.9 μM) Eg5 inhibitor-binding pocket. This second value is an estimate as the concentrations of BI8 and protein are too low to accurately estimate the true value and it could therefore be significantly higher and the limiting solubility of BI8 prevents a suitable experimental setup to obtain a more accurate value. Subsequent injection of ispinesib to the preformed Eg5-BI8 complex showed that ispinesib could bind to Eg5 with a ratio of 1:1, consistent with it replacing BI8 from one binding site only, probably the overlapping site (helix α2/loop L5/helix α3) (Figure 4f).

The reverse experiment showed that after injection of ispinesib (Figure 4g), BI8 could still bind to the preformed Eg5-ispinesib complex with a binding stoichiometry of 1:1 (Figure 4h). The data indicate that because the first allosteric binding pocket (helix α2/loop L5/helix α3) is occupied by ispinesib, BI8 with its significantly higher K_d value can only bind to the second, still unoccupied inhibitor-binding pocket (helices α4 and α6). The K_d for this binding event is 3.3 μM, and although not in exact agreement with either of the values obtained when titrating BI8 alone, we suggest that this corresponds to the site with the lower dissociation constant of 0.65 μM since affinity at the weaker site is not possible even to estimate accurately with ITC. Therefore, the physiologically relevant site is the novel allosteric pocket. The stoichiometry of binding (n), K_d values, entropic and enthalpic values are

dx.doi.org/10.1021/ja310377d | *J. Am. Chem. Soc.* 2013, 135, 2263–2272

represented in Figure 4i. To add more evidence to this conclusion, two further orthogonal techniques were used.

Surface Plasmon Resonance Analysis of BI8 Binding to Eg5. A similar ispinesib blockade approach was used to distinguish binding affinities for BI8 at the two sites using SPR (Figure 5a–f). First, monastrol/ispinesib control experiments were carried out to demonstrate the validity of this approach. Then, two-site binding to Eg5 by BI8 was demonstrated by a series of BI8 injections with a maximum concentration of 0.528 mM. Fitting the data with a steady state affinity model generated K_d values of 470 nM and ~34 μM, respectively (Figure 5g) comparable to the affinities estimated from ITC measurements (Figure 4i). The ispinesib site was then blocked by injection with 10 μM ispinesib and subsequent extended periods of injection with ispinesib-free buffer demonstrated a very slow dissociation from Eg5, resulting in this site being blocked for the duration of subsequent experiments. BI8 injection following ispinesib binding showed a maximal response approximately half that seen in the initial experiment without ispinesib, indicating a 1:1 stoichiometry. Fitting the data with a one site steady-state affinity model resulted in a K_d of 640 nM, similar to the more potent of the two values measured in the absence of ispinesib and to the more potent value observed in ITC.

Eg5 Has One Tight Binding Site for BI8 That Can Be Detected by Quenching of Intrinsic Fluorescence. Ispinesib quenches the intrinsic fluorescence of Eg5[20] as illustrated by the spectra in Figure 6a. Titration of the fluorescence of Eg5 with ispinesib-serves as a control for tight binding with a stoichiometry of 1:1 (Figure 6b, squares) using excitation at 280 nm and emission at 380 nm. At an Eg5 concentration of 6.4 μM, ispinesib titrates with an equivalence point at 8.4 μM that is in reasonable agreement with the concentration of 6.4 μM determined by the Bradford assay. Figure 6a also indicates that BI8 significantly quenches the fluorescence of Eg5 at emission wavelengths <370 nm, but has little effect at longer wavelengths. The decrease in fluorescence emission at 310 nm can be used to titrate BI8 binding to Eg5 (Figure 6b, diamonds). An unrestrained fit to a full mutual depletion model with one site yielded an Eg5 concentration, K_d and maximum decrease of 7.5 μM, 0.71 μM and 60%, respectively. This establishes a 1:1 stoichiometry for tight binding of BI8, but cannot provide a fully accurate K_d because of the high degree of mutual depletion and the uncertain partial contribution of binding of BI8 to the weaker site. The weaker site for BI8 that is observed by ITC apparently does not titrate in this range, although the continued slow decrease in fluorescence at higher BI8 concentration may represent increasing partial occupancy of the weak site. At a lower Eg5 concentration of 1.07 μM Eg5, the influence of mutual depletion is decreased and the fit yields an Eg5 concentration and K_d of 0.96 and 0.34 μM, respectively (Figure 6b insert).

The decrease in fluorescence on BI8 binding can also be used to determine the rate constant, k_{on}, for BI8 binding by stopped flow. Mixing Eg5 with an excess of BI8 produces a rapid decrease in intrinsic fluorescence that obeys first-order kinetics. The observed rate increases linearly with BI8 concentration (Figure 6c) with a slope of 0.24 M^{-1} s^{-1} that defines the bimolecular association rate constant for binding of BI8 to the tight site. The rate of BI8 dissociation can be calculated as ~0.14 s^{-1} using $K_d = k_{off}/k_{on}$ and values of 0.34 μM and 0.24 M^{-1} s^{-1} for K_d and k_{on}, respectively. The intercept in Figure 6c is plotted at this value of 0.14 s^{-1}, but the intercept is not significantly different from zero by extrapolation. Additionally, preloading of BI8 at the tight site has little effect on the rate of ispinesib binding (Figure 6d)

4. DISCUSSION

The crystal structure of the Eg5-ADP-BI8 complex reveals a second druggable inhibitor binding pocket ~19 Å from the extensively studied allosteric ispinesib site. The existence of this site, located between helices α4 and α6 of the Eg5 motor domain, has previously been proposed for biaryl Eg5 inhibitors using biochemical and modeling techniques.[6,7] These biaryl inhibitors have the unusual property of being both allosteric and competitive with ATP. This is in marked contrast to the BI8 class of benzimidazole inhibitors that have been shown to be uncompetitive with ATP. It would be of considerable interest to obtain detailed structural information on the binding of biaryl inhibitors to determine how these two classes of inhibitors can bind to the same region on Eg5, yet alter the kinetics in such different ways, however biaryl compounds do not seem to bind to Eg5 in the absence of MTs. The existence of a similar site (and other putative novel binding pockets) has also been suggested using molecular modeling simulations.[8] We now provide the structural basis for this pocket and a detailed understanding of the Eg5-inhibitor interactions. Unexpectedly, inhibitor binding was also observed in the ispinesib site, but using three orthogonal biophysical and biochemical techniques, we have shown that there is a single high affinity site, that high-affinity binding is the result of binding to the α4/α6 site, and that this site is responsible for the observed inhibition. High affinity binding at this site appears to be driven by both a network of aromatic interactions and hydrogen bonding with the carboxylate group of BI8. These interactions are much less prominent in the second pocket, perhaps explaining the weaker electron density and lower affinity of the inhibitor at this site.

The binding mode of ispinesib and other allosteric inhibitors to the pocket formed by helix α2/loop L5/helix α3 and the sequence of structural changes leading to the final inhibitor bound state have been revealed in considerable detail using steady state and presteady state kinetics as well as biophysical and structural methods.[18−23] The location of the site between helices α4 and α6 immediately suggests a mechanism for the inhibitory effect of the compound. Small changes in the nucleotide-binding pocket induced by ATP hydrolysis are thought to lead to amplified structural changes in the switch II cluster and neck-linker region which generate the molecular motion responsible for shifting the two antiparallel MTs apart to form the bipolar spindle. By binding between helix α4 of the switch II cluster and helix α6 preceding the neck-linker, BI8 may lock Eg5 in a conformation that is no longer able to undergo the nucleotide-dependent conformational changes required for the completion of the catalytic cycle. The mechanism by which this inhibitor can exert its physiological effect on ATPase activity is emphasized by molecular dynamics simulations, which demonstrated that residues in this pocket directly interact with loop L13. This loop is highly correlated with the Switch-I and Switch-II regions whose movement is critical allowing movement of the neck linker region. Furthermore, the neck linker region in the Eg5-BI8 complex is locked in the intermediate state that was also observed for inhibitors binding in the ispinesib allosteric binding pocket.[22] In the Eg5-STLC complex, the transition from the native to the inhibitor bound conformation goes through a sequence of structural changes from the native state without inhibitor to the

intermediate state in which helix $\alpha4$ is in the obstructive position and as a consequence the neck-linker is undocked. Finally, in the final inhibitor-bound state, the switch II cluster is in the permissive position allowing the neck linker to dock to the motor domain from the initial perpendicular orientation that involves the swinging of the neck-linker of about 32 Å.[21] Although allosteric inhibitors such as ispinesib, monastrol, and STLC as opposed to BI8 target two distinct sites on Eg5, these complexes reveal the same intermediate state; in both complexes, ADP-release is inhibited and the monoastral spindle phenotype is observed in cells. Therefore, we hypothesize that inhibitors like BI8, which target a different site, act through a similar mechanism. Further investigations will be necessary to provide insights into the sequence of conformational changes occurring in the catalytic domain in support to our hypothesis.

5. CONCLUSION

This structural characterization of the $\alpha4/\alpha6$ inhibitor-binding site in Eg5, coupled with the previous identification of the benzimidazole series of inhibitors, creates the opportunity for both structure-based and ligand-based approaches to develop novel inhibitor series for Eg5. The significant conformational changes on ligand binding generate a well-defined "druggable" pocket and the crystal structure now enables the application of structure-based design and screening approaches. Importantly, the development of inhibitors at this site has the potential for delaying the onset of resistance to drugs targeting the ispinesib site. This could be particularly relevant since mutants highly resistant to ispinesib treatment have been observed in cell culture and combination therapy is a well-established approach to slow down the onset of resistance. With the existing benzimidazole inhibitors demonstrating inhibition of the ATPase activity in the nanomolar range, this is an exciting possibility toward the development of new drug candidates.

Abbreviations. BI8, benzimidazole number 8; CENP-E, centromere-associated protein E; ITC, isothermal titration calorimetry; KSP, kinesin spindle protein; MT, microtubule; SPR, Surface Plasmon Resonance.

■ ASSOCIATED CONTENT

Supporting Information

Synthesis of BI8; cloning, expression and purification of Eg5 constructs; data collection and refinement; isothermal titration calorimetry. This material is available free of charge via the Internet at http://pubs.acs.org.

■ AUTHOR INFORMATION

Corresponding Author

f.kozielski@beatson.gla.ac.uk; ddh@andrew.cmu.edu

Present Address

[†]School of Chemical and Biotechnology, SASTRA University, Tirumalaisamudram, Thanjavur 613401, Tamilnadu, India.

Author Contributions

[‡]These authors contributed equally.

Notes

The authors declare no competing financial interest.

■ ACKNOWLEDGMENTS

We thank Diamond Light Source for access to beamlines I02 (MX6683) and I03 that contributed to the results presented here. We are grateful to Prof. Alan Cooper for his insightful comments on ITC and Dr. Marta Dozynkiewicz for her support during SPR experiments. This project was supported by CR-UK.

■ REFERENCES

(1) Beer, T. M.; Goldman, B.; Synold, T. W.; Ryan, C. W.; Vasist, L. S.; Van Veldhuizen, P. J., Jr.; Dakhil, S. R.; Lara, P. N., Jr.; Drelichman, A.; Hussain, M. H.; Crawford, E. D. *Clin. Genitourin. Cancer* **2008**, *6*, 103−109.

(2) Burris, H. A., III; Jones, S. F.; Williams, D. D.; Kathman, S. J.; Hodge, J. P.; Pandite, L.; Ho, P. T.; Boerner, S. A.; Lorusso, P. *Invest. New Drugs* **2011**, *29*, 467−472.

(3) Wood, K. W.; Lad, L.; Luo, L.; Qian, X.; Knight, S. D.; Nevins, N.; Brejc, K.; Sutton, D.; Gilmartin, A. G.; Chua, P. R.; Desai, R.; Schauer, S. P.; McNulty, D. E.; Annan, R. S.; Belmont, L. D.; Garcia, C.; Lee, Y.; Diamond, M. A.; Faucette, L. F.; Giardiniere, M.; Zhang, S.; Sun, C. M.; Vidal, J. D.; Lichtsteiner, S.; Cornwell, W. D.; Greshock, J. D.; Wooster, R. F.; Finer, J. T.; Copeland, R. A.; Huang, P. S.; Morgans, D. J., Jr.; Dhanak, D.; Bergnes, G.; Sakowicz, R.; Jackson, J. R. *Proc. Natl. Acad. Sci. U.S.A.* **2010**, *107*, 5839−5844.

(4) Blagden, S. P.; Molife, L. R.; Seebaran, A.; Payne, M.; Reid, A. H.; Protheroe, A. S.; Vasist, L. S.; Williams, D. D.; Bowen, C.; Kathman, S. J.; Hodge, J. P.; Dar, M. M.; de Bono, J. S.; Middleton, M. R. *Br. J. Cancer* **2008**, *98*, 894−899.

(5) Yan, Y.; Sardana, V.; Xu, B.; Homnick, C.; Halczenko, W.; Buser, C. A.; Schaber, M.; Hartman, G. D.; Huber, H. E.; Kuo, L. C. *J. Mol. Biol.* **2004**, *335*, 547−554.

(6) Luo, L.; Parrish, C. A.; Nevins, N.; McNulty, D. E.; Chaudhari, A. M.; Carson, J. D.; Sudakin, V.; Shaw, A. N.; Lehr, R.; Zhao, H.; Sweitzer, S.; Lad, L.; Wood, K. W.; Sakowicz, R.; Annan, R. S.; Huang, P. S.; Jackson, J. R.; Dhanak, D.; Copeland, R. A.; Auger, K. R. *Nat. Chem. Biol.* **2007**, *3*, 722−726.

(7) Parrish, C. A.; Adams, N. D.; Auger, K. R.; Burgess, J. L.; Carson, J. D.; Chaudhari, A. M.; Copeland, R. A.; Diamond, M. A.; Donatelli, C. A.; Duffy, K. J.; Faucette, L. F.; Finer, J. T.; Huffman, W. F.; Hugger, E. D.; Jackson, J. R.; Knight, S. D.; Luo, L.; Moore, M. L.; Newlander, K. A.; Ridgers, L. H.; Sakowicz, R.; Shaw, A. N.; Sung, C. M.; Sutton, D.; Wood, K. W.; Zhang, S. Y.; Zimmerman, M. N.; Dhanak, D. *J. Med. Chem.* **2007**, *50*, 4939−4952.

(8) Zhang, W. *J. Phys. Chem. B* **2011**, *115*, 784−795.

(9) Sheth, P. R.; Shipps, G. W., Jr.; Seghezzi, W.; Smith, C. K.; Chuang, C. C.; Sanden, D.; Basso, A. D.; Vilenchik, L.; Gray, K.; Annis, D. A.; Nickbarg, E.; Ma, Y.; Lahue, B.; Herbst, R.; Le, H. V. *Biochemistry* **2010**, *49*, 8350−8358.

(10) Lahue, B. R.; Ma, Y.; Shipps, G. W., Jr.; Seghezzi, W.; Herbst, R. *Bioorg. Med. Chem. Lett.* **2009**, *19*, 3405−3409.

(11) Kabsch, W. *Acta Crystallogr., Sect. D: Biol. Crystallogr.* **2010**, *66*, 125−132.

(12) Vagin, A. A.; Isupov, M. N. *Acta Crystallogr., Sect. D: Biol. Crystallogr.* **2001**, *57*, 1451−1456.

(13) Murshudov, G. N.; Vagin, A. A.; Dodson, E. J. *Acta Crystallogr., Sect. D: Biol. Crystallogr.* **1997**, *53*, 240−255.

(14) Adams, P. D.; Afonine, P. V.; Bunkoczi, G.; Chen, V. B.; Davis, I. W.; Echols, N.; Headd, J. J.; Hung, L. W.; Kapral, G. J.; Grosse-Kunstleve, R. W.; McCoy, A. J.; Moriarty, N. W.; Oeffner, R.; Read, R. J.; Richardson, D. C.; Richardson, J. S.; Terwilliger, T. C.; Zwart, P. H. *Acta Crystallogr., Sect. D: Biol. Crystallogr.* **2010**, *66*, 213−221.

(15) Emsley, P.; Lohkamp, B.; Scott, W. G.; Cowtan, K. *Acta Crystallogr., Sect. D: Biol. Crystallogr.* **2010**, *66*, 486−501.

(16) Schuettelkopf, A. W.; van Aalten, D. M. *Acta Crystallogr., Sect. D: Biol. Crystallogr.* **2004**, *60*, 1355−1363.

(17) *The PyMOL Molecular Graphics System*, Version 1.5.0.4, Schrödinger, LLC., 2010.

(18) Luo, L.; Carson, J. D.; Dhanak, D.; Jackson, J. R.; Huang, P. S.; Lee, Y.; Sakowicz, R.; Copeland, R. A. *Biochemistry* **2004**, *43*, 15258−15266.

(19) Talapatra, S. K.; Schüttelkopf, A. W.; Kozielski, F. *Acta Crystallogr., Sect. D: Biol. Crystallogr.* **2012**, *68*, 1311−1319.

(20) Lad, L.; Luo, L.; Carson, J. D.; Wood, K. W.; Hartman, J. J.; Copeland, R. A.; Sakowicz, R. *Biochemistry* **2008**, *47*, 3576−3585.

(21) Maliga, Z.; Xing, J.; Cheung, H.; Juszczak, L. J.; Friedman, J. M.; Rosenfeld, S. S. *J. Biol. Chem.* **2006**, *281*, 7977−7982.
(22) Kaan, H. Y.; Ulaganathan, V.; Hackney, D. D.; Kozielski, F. *Biochem. J.* **2009**, *425*, 55−60.
(23) Sheth, P. R.; Basso, A.; Duca, J. S.; Lesburg, C. A.; Ogas, P.; Gray, K.; Nale, L.; Mannarino, A. F.; Prongay, A. J.; Le, H. V. *Biochemistry* **2009**, *48*, 11045−11055.